12

Active Isolation and Damping of Vibrations for High Precision Laser Cutting Machine

Andrea Tonoli[1,2], Angelo Bonfitto[2] and Mario Silvagni[2],
Lester D. Suarez[2] and Enrico Zenerino[2]
[1]Mechanics Department
[2]Mechatronics Laboratory – Politecnico di Torino
Italy

1. Introduction

High precision industrial machines suffer the presence of vibrations due to several noise sources: ground vibration, acoustic noise, direct force disturbances. These are sources of several problems at different levels and of different natures causing the performance losses on sensitive systems (Crede, 1951), (Rivin, 1979).
In the last years the need of higher processing quality and throughput resulted in a continuing demand for higher accuracy. Therefore active isolation and vibration damping systems became mandatory to satisfy these requests (Preumont, 2002), (Hyde, 1997).
In general, machine supports are designed for high stiffness to obtain a robust machine alignment with respect to its surroundings. However, in the presence of significant ground vibration levels the support stiffness is commonly sacrificed to reduce the transmission to the payload stage. Efforts to go towards these issues are recorded in several applications and the solutions are different for any particular situation, depending on the nature of the vibration sources, the amount of the disturbances and the machine environment.
Three main categories of possible approaches can be identified: passive, active and semi-active configurations.
Completely passive solutions have almost reached their maximum potential which is still not sufficient to satisfy stringent requirements. On the opposite, the exponential growth in electronics and actuators fields made the use of active and semi-active isolation more feasible. In particular, active control architectures allow to perform an effective isolation at low frequencies, which is a common requirement for very demanding applications like micrometer motion control, defect inspections, critical dimensions measurement and overlay metrology.
Active control arrangements are provided with sensors, actuators and controllers (Watters, 1988). Each of them can be classified depending on their technology and physical working principle. For the application considered in this work, the main categories of sensors used are: displacement, velocity, acceleration, strain and force. In the same way, the most common types of actuators are: shape memory alloys, magnetic, piezoelectric, magnetostrictive and magneto-rheological fluids actuators (Thayer, 1998). The choice of sensors and actuators is strictly related to the type of application and requirements and has also influence on the selection of the control strategies to be

applied. Typically the main control approaches are feedback, classical or model based, and feed-forward technique, mostly with adaptive filtering of reference (Anderson, 1996). Depending on the type of the controller, the system model can be used to support the control design or can play itself a fundamental role on the control action (model based strategies) (Beadle et al, 2002), (Sullivan, 1997).

This chapter is focused on the evaluation of an active isolation and vibration damping device on the working cell of a micro-mechanical laser center, using active electromagnetic actuators. To clarify the goal of this study it is important to point out that: a) the vibration damping is defined as the reduction of the response amplitude of the system within a limited bandwidth near the natural frequencies of the system; b) vibration isolation is defined as the attenuation of the response of the system after its corner frequency to cut-off all disturbances after that frequency allowing all signals below it to pass with no alterations.

The machine object of study is composed by two main parts: a frame support and a payload stage where the laser cutting is performed. The system performance in terms of accuracy and precision is reduced by the presence of two main vibration sources: the ground and the stage itself. The active device should meet two main goals: the payload vibrations damping and the reduction of the transmissibility of ground disturbances.

In this work the phases followed to design, realize and validate the device are illustrated with a particular emphasis on the mechatronics aspects of the project.

A detailed analysis of the plant components is reported along with an exhaustive explanation of the supports, actuation and sensing subsystems design criteria.

The actuation block consists in four electromagnetic Lorentz type actuators (two per axis) (Brusa, 2001). The absolute velocities of the frame support and of the stage are measured by means of eight geophone sensors to determine the amount of the disturbances (Huan, 1985), (Riedesel, 1990). The considerations leading to the choice of this sensing system are reported along with the related signal conditioning stage. The design of the supports between the ground and the frame and of the connections between the frame and the stage is also explained.

Furthermore, all the subsystems described in the first part of the chapter are modeled along with their interactions. The Lagrange equations approach is used to represent the system behavior and in particular the links between the mechanical and electrical subsystems are illustrated. The model includes the plant, the sensing, the control and the actuation blocks. In particular, the mechanical subsystem is considered as a four degrees of freedom system. Time and frequency domain computations are carried out from the model to evaluate vibration levels and displacements and to identify which control parameters need to be carefully designed to satisfy the requirements.

The last section gives details about the proposed control action and the validation of the device. The control law consists in a couple of decentralized actions exerted along X and Y -axis allowing to minimize the ground vibrations transmission and damp the payload vibrations. A Lead-Lag control strategy, performed with a digital platform based on DSP and FPGA, is used to compensate the high-pass band dynamic of the geophone sensors and to damp the vibrations (Kuo, 1996), (Elliott, 2001). The payload isolation is achieved by feeding the control block with the difference of frame and stage velocities and giving the proper current command to the actuators.

The chapter concludes on the comparisons between simulation and experimental tests, illustrating the validity of the model and the effectiveness of the proposed approach. In particular, the performance of the vibration damping has been evaluated by using the frequency responses between the actuators force and the payload velocities and the active

isolation by simulating numerically the disturbances coming from the ground and by evaluating their transmission through all the system till the payload in closed loop configuration.

2. System architecture

In this section of the chapter a full description of all the machine subsystems is provided. The mechanical, electrical, electronic and control parts are identified and fully described separately in the first part. Furthermore, since the project can be assumed as a classical mechatronics application, the different blocks are analyzed in their interactions in order to provide an overall view of the system.

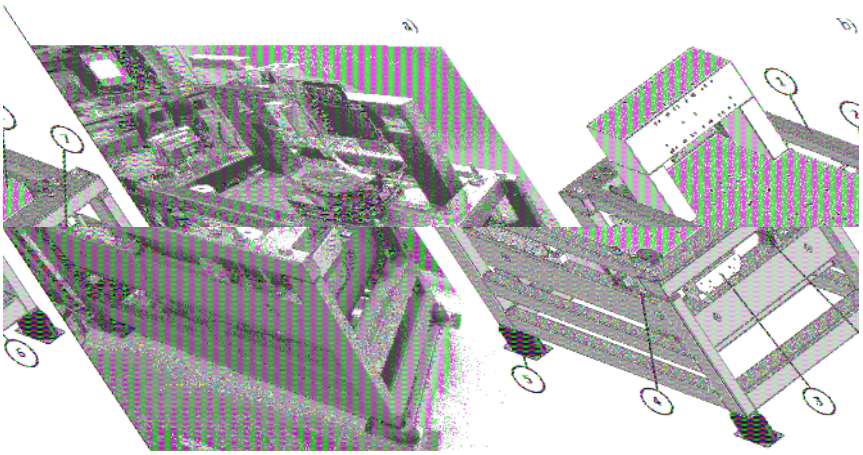

Fig. 1. a) Picture of the machine. b) Sketch of the system. 1: Frame; 2: Stage (Payload); 3: Actuators; 4: Frame – Stage Springs; 5: Air springs; 6: Frame sensors; 7: Stage sensors.

Figure 1.a shows a picture of the laser cutting machine while in the sketch of Figure 1.b all the components of the system are highlighted. The stage (payload) (2) consists in a granitic base that can move freely within the work volume and is surrounded by four electromechanical actuators (3) acting between the frame (1) and the stage. The machine is partially isolated from the ground by means of four air springs (5). Four mechanical springs (4) are vertically placed between the frame and the stage. The vibrations due to the machine process and coming from the ground are measured on the payload and on the frame by means of eight velocity inertial sensors (6, 7). A schematic representation of the actuators, sensors and springs position is reported in Figure 2 where c_{GF} and k_{GF} represent the damping and the stiffness introduced by the supports, c_{FS} and k_{FS} are the damping and the stiffness of the springs acting as connections between the frame and the stage. Actuators and sensors are placed so that they can be considered collocated in order to minimize the couplings between the axes actions by keeping the proper alternation between resonances and anti-resonances in the system dynamics. The main machine parameters and specifications are listed in Table 1.
The design phases have been performed considering the mechatronics nature of the system and the interactions between the machine subsystems, illustrated in Figure 3. A classical

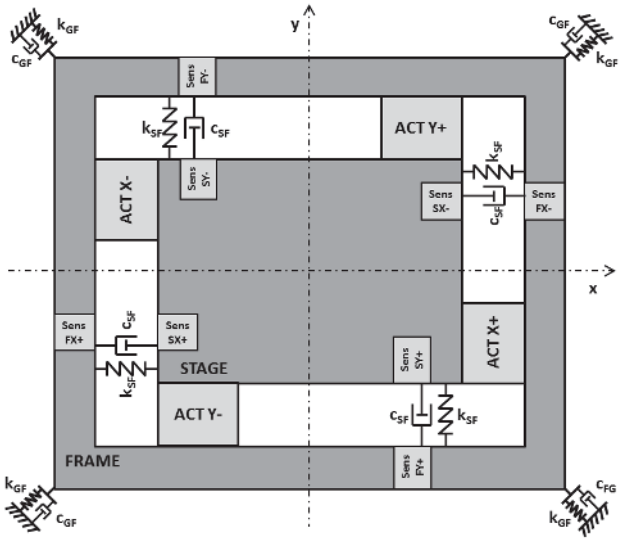

Fig. 2. XY plane view of the system. Frame-stage spring (k_{FS} , c_{FS}), electromagnetic actuator (ACT), velocity sensor (Sens.), Frame-Ground spring (k_{FG} , c_{FG}).

Stage mass	1450 kg
Frame mass	300 kg
Maximum displacement of the stage	2.5 mm
Inertia of the stage along X -axis in YZ -plane	200 kg m^2
Inertia of the frame along X -axis in YZ -plane	100 kg m^2

Table 1. Main parameters and specifications of the machine.

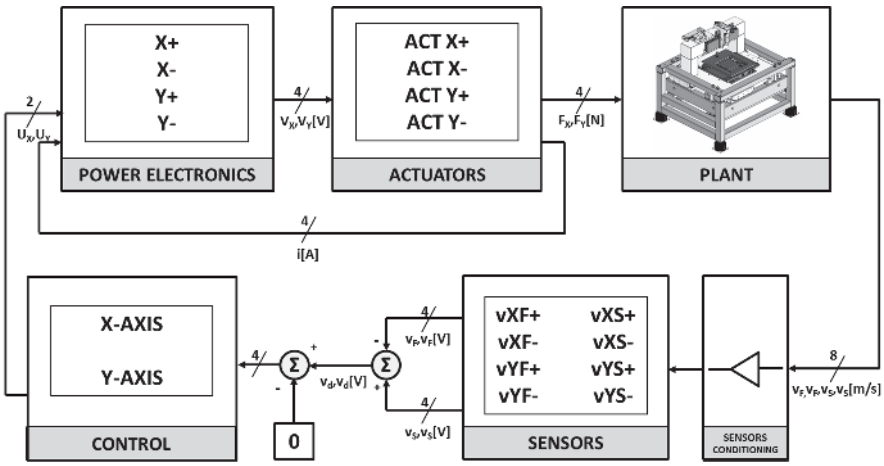

Fig. 3. Block diagram of the system.

feedback behavior is performed: eight velocities are acquired by the sensors measurements and elaborate with conditioning and filtering stages in order to feed the actuators with the proper commands by means of power electronics action. The filtering stage consists in the implementation of a Lead-Lag control strategy designed to fulfill the machine requirements in terms of: a) active isolation from the disturbances coming from the ground and b) damping of the vibrations generated by the machine processes.

2.1 Actuators subsystem

The actuation on the system is realized by means of four electromagnetic Lorentz type actuators placed as illustrated in Figure 1 and Figure 2.
The actuator configuration is reported in Figure 4 (a) Picture, b) Sketch), A and B are two permanent magnets while C indicates the coil.

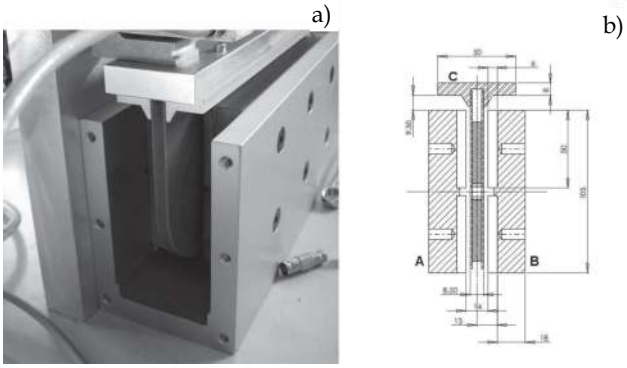

Fig. 4. a) Picture of the actuator, b) Section view (A and B: permanent magnets, C:coil).

The force F_{ACT} generated by each actuator is:

$$F_{ACT} = BNli \tag{1}$$

where B is the magnetic field, N is the number of turns, i is the current flowing in the coil, l is the coil length. The direction of the resulting force is illustrated in Figure 5. The amount of required force for each actuator is equal to 200 N while the main parameters of the designed actuator are reported in Table 2.

Coil thickness	6	mm
Coil length	3.3	mm
Coil active section	198	mm^2
Copper current density	12	A/mm^2
Coil length (l)	200	mm
Coil max actuation force (F_{ACT})	200	N
Number of turns (N)	263	-
Number of coils per axis	2	-

Table 2. Actuators main parameters.

The design of the actuators has been performed starting from the requirements of force and maximum displacement of the stage, then a current density and the wire section have been selected in order to perform a FEM analysis and to compute the magnetic field. Finally, once known all the electrical parameters, the coil length l has been computed.

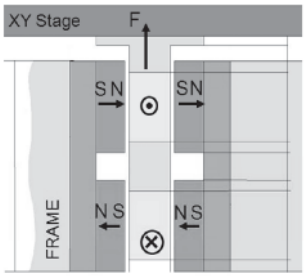

Fig. 5. Actuator force generation.

The actuators parameters have been identified experimentally. The resulting values are: resistance $R = 4.33\ \Omega$, $R = 9.64\ mH$. The actuator transfer function can be expressed as:

$$G_{ACT}(s) = \frac{1}{Z(s)} = \frac{1}{sL + R} = \frac{\frac{1}{L}}{s + \frac{R}{L}} \tag{2}$$

The stationary gain $G(s = 0)$ is:

$$G(s = 0) = 20\log_{10}\left(\frac{1}{R}\right) = -12.73\ dB \tag{3}$$

The electrical pole ω_e is:

$$\omega_e = \frac{R}{L} = 449\ \ rad/s = 72\ Hz \tag{4}$$

The resulting actuator trans-conductance transfer function is reported in Figure 6.

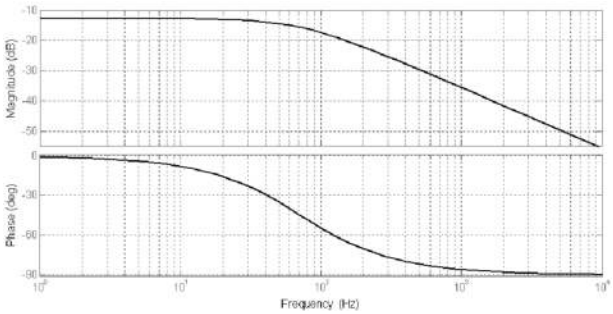

Fig. 6. Actuator trans-conductance transfer function (magnitude and phase).

2.2 Springs and supports

The frame and the stage are connected in the vertical direction by means of four linear springs placed as indicated by 4 in Figure 1 (c_{SF} and k_{SF} in Figure 2). The design has been performed computing displacements and stresses with a FEM software, starting from the following requirements:

- infinite fatigue life;
- stiffness $\begin{cases} k_{SFx} = 40\,N/mm; \\ k_{SFy} = 40\,N/mm; \\ k_{SFz} = 32500\,N/mm; \end{cases}$
- damping $\begin{cases} c_{SFx} = 228\,Ns/m; \\ c_{SFy} = 228\,Ns/m; \\ c_{SFz} = 4313\,Ns/m; \end{cases}$
- maximum displacement $z_{MAX} = 2.5mm;$

The designed spring is made of harmonic steel and is characterized by:

- length $l_{SPRING} = 125mm;$
- diameter $d_{SPRING} = 5mm;$
- maximum value of stress $\sigma_{MAX} = 500MPa.$

The supports chosen to provide the system with a partial level of isolation from the ground are four air-springs (5 in Figure 1, k_{GF} and c_{GF} in Figure 2) consisting in resilient element air and neoprene diaphragm. They are characterized by the following features:

- Nominal natural frequency: $\begin{cases} f_{GFx} = 12.3Hz; \\ f_{GFy} = 12.3Hz; \\ f_{GFz} = 5.4Hz; \end{cases}$
- stiffness $\begin{cases} k_{GFx} = 450\,N/mm; \\ k_{GFy} = 450\,N/mm; \\ k_{GFz} = 500\,N/mm; \end{cases}$
- damping $\begin{cases} c_{GFx} = 575\,Ns/m; \\ c_{GFy} = 575\,Ns/m; \\ c_{GFz} = 1700\,Ns/m; \end{cases}$
- Transmissibility at resonance: 8:1;
- The maximum load is equal to 545 kg;
- The maximum air pressure is equal to 80 psi (5.5 bar).

2.3 Sensing subsystem

The disturbances on the plant are evaluated by measuring the velocities on the stage and on the frame along X-axis and Y-axis by means of eight geophones placed as indicated in Figure 2. They can be considered as the most common velocity inertial sensors to measure seismic vibrations and can be classified as electromagnetic sensors that measure the velocity and produce a voltage signal thanks to the motion of a coil in a magnetic field (Hauge et al,

2002). One configuration of the conventional geophones consists of a cylindrical magnet coaxial with a cylindrical coil as shown in Figure 7. The coil is made up of a good conductor like copper and is wound around a nonconductive cylinder to avoid the effect of the eddy current that can be caused by the current induced in the coil. The wire diameter and the dimensions of the holding cylinder are designed according to the application requirements.

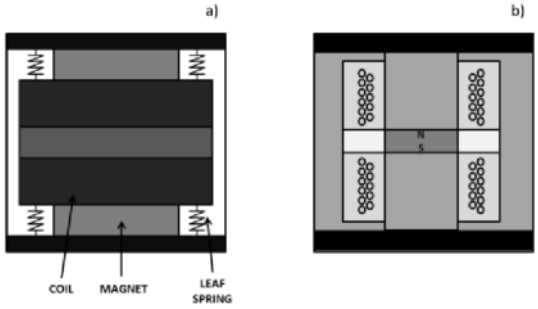

Fig. 7. Geophone active configuration scheme. a) Coil and springs installation. b) Cross section.

The internal core is a permanent magnet selected to give the highest possible magnetic field density to maximize the induced voltage in the coil. The coil is attached to the casing of the geophone by means of leaf springs (membranes); these springs are designed so as to maintain alignment in the motion of the coil relative to the magnet keeping the lowest stiffness possible in order to have a low resonant frequency for the geophone.
The reverse configuration (Figure 8) is realized using a coil fixed to the casing while the moving mass is the permanent magnet. Since the mass of the magnet is heavier than that of the coil, this configuration leads to a lower natural frequency, but the moving part is larger and heavier.

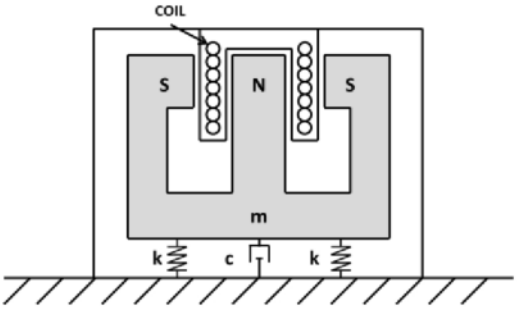

Fig. 8. Geophone reverse configuration scheme.

Two geophone sensors are tested in the system: active sensor LF24 (configuration in Figure 8) and passive sensor SM6 (configuration in Figure 7). The LF-24 Low Frequency Geophone is characterized by the following parameters: natural frequency at 1Hz, distortion measurement frequency at 12Hz and sensitivity equal to 15V/(m/s).
The sensor chosen is the passive sensor SM6 because it allows to have an extreme low noise though the output needs to be amplified by an active conditioning stage

The transfer function of the sensor response between the velocity of the casing and the induced voltage in the coil can be written in the form

$$TFG = -\frac{Gs^2}{s^2 + 2\xi\omega_n + \omega_n{}^2} \tag{5}$$

where $\omega_n = \sqrt{K/m}$ is the natural frequency of the geophone, $\xi = C/2m\omega_n$ is the damping ratio including the effect of the eddy current and $G = Bl$ is the transduction constant, where B is the magnetic field generated by the permanent magnet and l is the length of the coil.
Considering that the first natural frequency of the system is at about 1.8 Hz, close to the geophone natural frequency, the sensor sensitivity cannot be simply modeled as a constant value. Thus the transfer function of the geophone response must be identified to make the result more reliable.

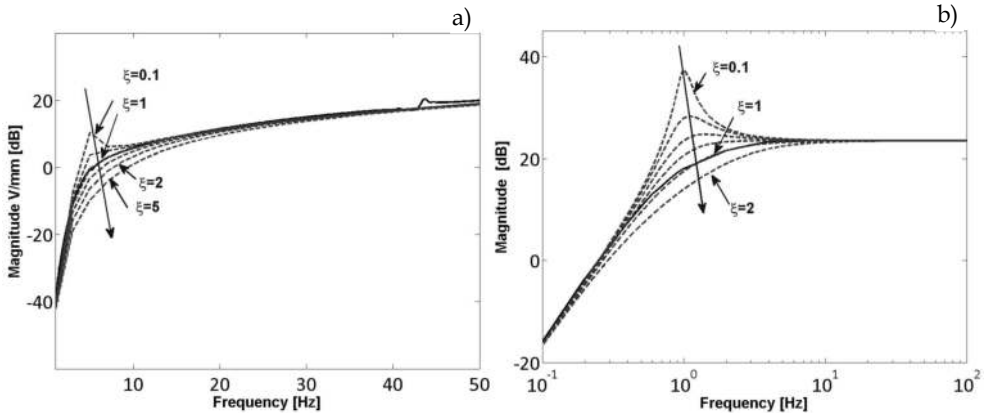

Fig. 9. Geophone damping ratio identification a) SM6 (Active configuration); b) LF24 (Reverse configuration).

SM6 is a passive velocity sensor with the following parameters: natural frequency is 4.5Hz, sensitivity is 28V/(m/s). The damping coefficient of SM6 can be indentified as the same way as LF24 in Figure 9.a and it is equal to 1.
Figure 9.b shows the LF24 transfer function expressed in Eq.5 identified experimentally. When the damping ratio is equal to 1, the experimental results fit quite well the model.
Since the generated voltage is proportional to the rate of crossing of the magnetic field, the output of the instrument will be proportional to the velocity of the vibrating body. A typical instrument of this kind may have a natural frequency between 1 Hz to 5 Hz. The sensitivity of such instrument may be in the range of 2 V/ms^{-1} to 3.5 V/ms^{-1} with the maximum displacement limited to about 5 mm peak to peak (Thomson, 1981). When a geophone is used to measure vibrations with a frequency below its natural frequency, the proof-mass tends to follow the motion of the vibrating body rather than staying stationary. This motion of the proof-mass following the casing reduces the relative motion which in turn reduces the induced voltage. Here the sensitivity of the sensor (ratio between the voltage and the casing velocity) becomes very small which restricts the performance of the sensor and limits the range of usage of the instrument to frequencies above its corner frequency. It is important to mention that

both displacement and acceleration can be obtained from the velocity sensor by means of the integral and derivative computation provided in most of the signal conditioner units.

2.4 Electronics subsystem

In this section the subsystems related to sensor acquisition and conditioning, power electronics and control implementation (Sensor conditioning, Power electronics, control blocks in Figure 3) are illustrated.

The electronics system architecture is shown in Figure 10. The main characteristic of this architecture is the serial communication input/output line that provides high noise immunity, which can be useful when signals must travel through a noisy environment, such as with remote sensors.

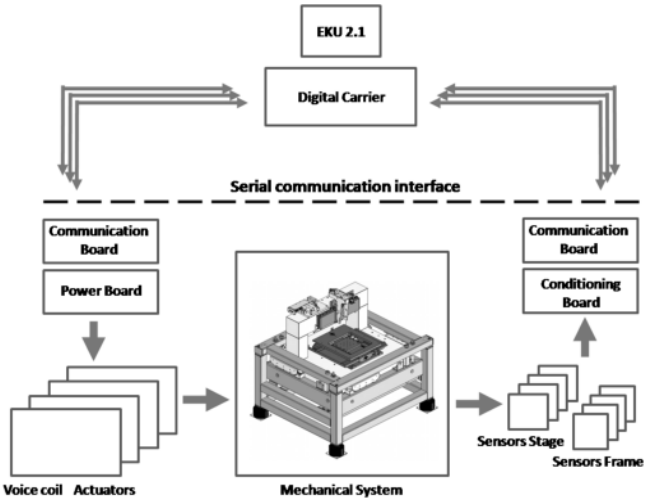

Fig. 10. Electronics subsystem.

The digital carrier is used like a buffer to provide the proper current level for the serial communication. Here, multiples system buses manage data exchange between the main serial communication core (FPGA) and the communication boards placed on the plant.

The communication boards are provided with one digital-to-analog converter (DAC) and two analog-to-digital converters (ADC). The DAC is a 16-bit, high-speed, low-noise voltage-output DAC with 30-MHz serial interface that is capable of generating output signal frequencies up to 1 MHz. The ADC is a single channel 12-bit analog-to-digital converter with a high-speed serial interface and sample rate range of 50 ksps to 200 ksps.

Control Unit (Control block in Figure 3)

The control module is supported by a DSP/FPGA–based digital control unit. Hence the overall control implementation can be divided between the two digital devices in order to fulfill different requirements: control strategy realization on DSP and serial communication implementation on FPGA.

The overall control strategy is characterized with a nested and decentralized control structure where only the outer loop is implemented on DSP while the inner loop (current loop) is realized on the power module directly. In particular, the outer loop computes the

right reference for the inner one starting from required error compensation. The same strategy is applied for each axis.

Sensors conditioning module (Sensor conditioning block in Figure 3)

The sensors conditioning module provides the output signal from geophone by means of an instrumentation amplifier circuits. The component is configured for dual-channel operation, in order to connect two geophones together. This conditioning circuit meets the needs of high performance and portable instrumentation when small signal amplitude conditioning brought out.

Figure 11, shows the circuit layout for dual-channel. R1A and R1B are the gain setting resistors.

With the ADC input in the range of [0-3] volt and assuming the maximum magnitude of noise on geophones measurement about 1000 m/s, the setting resistors are selected to achieve a gain of 100.

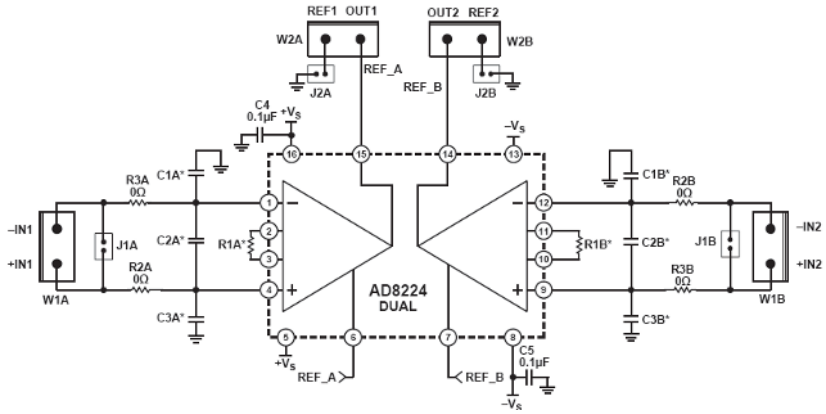

Fig. 11. Instrumentation amplifier circuits AD8224. R1A and R1B are the gain setting resistors.

Power electronics (Power electronics block in Figure 3)

The power module (Figure 12) is based on a trans-conductance amplifier instead of a switching amplifier in order to avoid noise due to the switching frequency. This kind of amplifier operates as a voltage-to-current converter whit a differential input voltage (voltage controlled current source configuration).

Figure 12 shows the electronics layout that is divided in three main stages: a) the trans-conductance amplifier (Trans Amp), b) the current amplifier (Curr Amp) and c) the feedback resistor (Feedback).

The power module uses the voltages reference (V_{in}) from the control unit to generate the proper current (I_L) to the load (electromagnetic actuator assumed as a RL load). The first stage performs the current control by means of an operational amplifier that is unity-gain stable with a bandwidth of 1.8MHz and it is internally protected against over-temperature conditions and current overloads. The second stage is a classical current amplifier with bipolar transistors in Darlington configuration to increase the current gain. The last stage provides the feedback signal to ensure the desired current in the load. The power supply is in the range of ±30V.

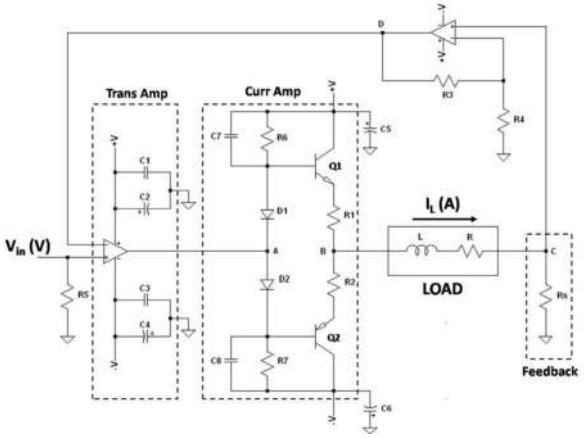

Fig. 12. Power electronic based on a trans-conductance amplifier.

3. Modeling

The system has been modeled by using four degrees of freedom considering that the dynamics along XZ and YZ planes are almost the same. As the vertical stiffness of the flexural springs is very high, it can be assumed that there is no relative displacement between stage and frame at vertical direction, which means the displacement in z axis about stage and frame are the same. Both the stage and the frame are assumed as moving about the frame mass center with the same rotating speed. Four flexural steel springs have been used to link the stage to the frame, four air springs are placed at the bottom of the frame, two actuators are working in series between the stage and the frame and two geophones are used to measure the velocities of stage and frame respectively. The model reference frames are defined in Figure 2 XY -plane view and in Figure 13, 16 YZ -plane view.

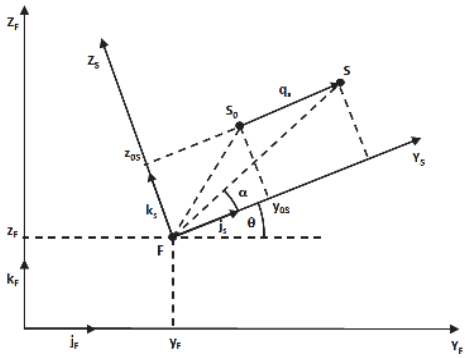

Fig. 13. YZ plane 4 dof kinematic relationships scheme.

The degrees of freedom of the model are:

$$\bar{X} = \left[y_F ; \quad z_F ; \quad \theta ; \quad q_S \right] \tag{6}$$

that indicate the displacement of the frame along Y-axis and Z-axis, the rotation of the frame (and stage) around the X-axis mass center and the stage displacement along its Y-axis.

Referring to the illustration in Figure 14, it is possible to obtain the formulation of the velocity of a generic point S of the stage:

$$\begin{aligned}\vec{V}_S &= \vec{V}_F + \dot{q}_S\vec{j}_S + \dot{\theta}FS\left[\cos\alpha\,\vec{k}_S - \sin\alpha\,\vec{j}_S\right] = \\ &= \dot{y}_F\vec{j}_F + \dot{z}_F\vec{k}_F + \left(\dot{q}_S - \dot{\theta}\,z_{0S}\right)\vec{j}_S + \dot{\theta}(y_{0S} + q_S)\vec{k}_S\end{aligned} \tag{7}$$

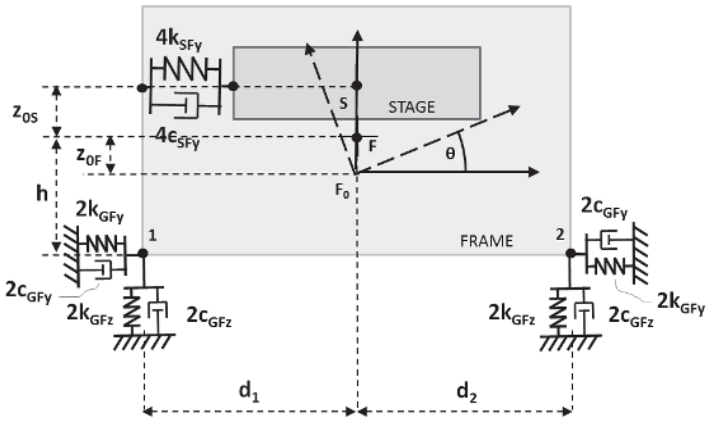

Fig. 14. YZ plane 4 dof model scheme.

The kinetic energy T of the system can be expressed as:

$$T = \frac{1}{2}m_S\vec{V}_S^{\,2} + \frac{1}{2}J_S\dot{\theta}^2 + \frac{1}{2}m_F\vec{V}_F^{\,2} + \frac{1}{2}J_F\dot{\theta}^2 \tag{8}$$

where m_S, m_F, J_S and J_F are the mass and the rotating inertia of the payload (the stage S) and of the frame F.

The potential energy U is obtained starting from the diagram reported in Figure 14:

$$\begin{aligned}U &= 2k_{GFz}\left(z_F - \theta d_1 - z_G\right)^2 + 2k_{GFy}(y_F + \theta h - y_G)^2 + 2k_{GFz}\left(z_F + \theta d_2 - z_G\right)^2 + \ldots \\ &+2k_{GFy}(y_F + \theta h - y_G)^2 + 2k_{SFy}q_S^{\,2}\end{aligned} \tag{9}$$

Owing to the Rayleigh dissipation formulation, the damping of the system is:

$$\begin{aligned}\Re &= 2c_{GFz}\left(\dot{z}_F - \dot{\theta} d_1 - \dot{z}_G\right)^2 + 2c_{GFy}(\dot{y}_F + \dot{\theta} h - \dot{y}_G)^2 + 2c_{GFz}\left(\dot{z}_F + \dot{\theta} d_2 - \dot{z}_G\right)^2 + \ldots \\ &+2c_{GFy}(\dot{y}_F + \dot{\theta} h - \dot{y}_G)^2 + 2c_{SFy}\dot{q}_S^{\,2}\end{aligned} \tag{10}$$

where each damping term c_i is obtained starting from the experimental identification of damping ratios ς_i:

$$c_i = 2\varsigma_i \sqrt{k_i m_i} \tag{11}$$

The inputs of the system are: the force of the electromagnet actuators F_{act}, the force of the stage F_S and the velocities from the ground in y direction v_{Gy} and z direction v_{Gz} v. The output are the velocities v_F of the frame and v_S of the stage measured with geophones sensors. Inputs and outputs are graphically represented in Figure 15.

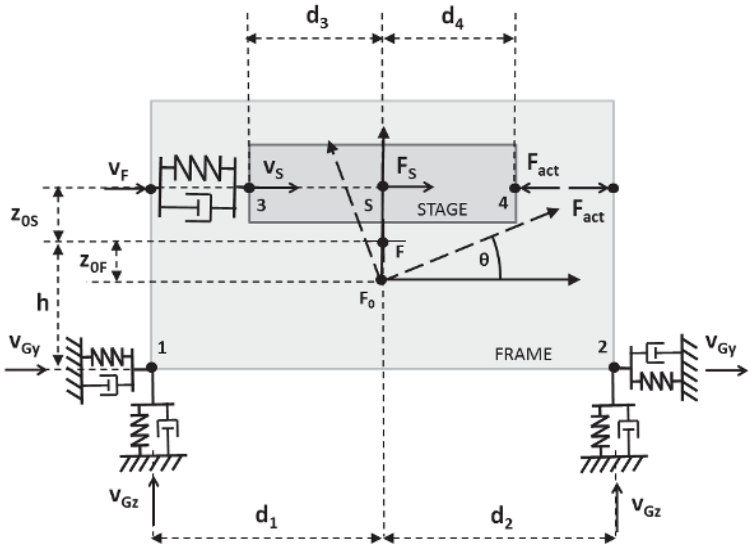

Fig. 15. YZ plane 4dof model scheme – input and output.

Using the Lagrange formulation is possible to write the equations of motion in the form:

$$\mathrm{M}\ddot{q} + C\dot{q} + \mathrm{K}q = \mathrm{T}\{F\} \tag{12}$$

where

$$q = \begin{pmatrix} y_F & z_F & \vartheta & q_S \end{pmatrix}^T \tag{13}$$

is the vector of the generalized coordinates,

$$F = \begin{pmatrix} v_{Gy} & v_{Gz} & F_S & F_{act} \end{pmatrix}^T \tag{14}$$

is the vector of the generalized forces and M is the mass matrix

$$M = \begin{bmatrix} m_{tot} & 0 & -m_S z_{0S} & m_S \\ 0 & m_{tot} & m_S y_{0S} & 0 \\ -m_S z_{0S} & m_S y_{0S} & J_{tot} & -m_S z_{0S} \\ m_S & 0 & -m_S z_{0S} & m_S \end{bmatrix} \tag{15}$$

with $m_{tot} = m_S + m_F$, $J_{tot} = J_S + J_F + m_S({y_{0S}}^2 + {z_{0S}}^2)$. y_{0S}, z_{0S} are the initial position of the stage. The matrix is symmetric and not diagonal because it takes into account the coupling between the stage and the frame dynamics.
The stiffness matrix K is:

$$K = \begin{bmatrix} 4k_{GFy} & 0 & 4k_{GFy}h & 0 \\ 0 & 4k_{GFz} & -2k_{GFz}d_1 + 2k_{GFz}d_2 & 0 \\ 4k_{GFy}h & -2k_{GFz}d_1 + 2k_{GFz}d_2 & 2k_{GFz}{d_1}^2 + 4k_{GFy}h^2 + 2k_{GFz}{d_2}^2 & 0 \\ 0 & 0 & 0 & 4k_{SFy} \end{bmatrix} \tag{16}$$

The damping matrix C is:

$$C = \begin{bmatrix} 4c_{GFy} & 0 & 4c_{GFy}h & 0 \\ 0 & 4c_{GFz} & -2c_{GFz}d_1 + c2_{GFz}d_2 & 0 \\ 4c_{GFy}h & -2c_{GFz}d_1 + 2c_{GFz}d_2 & 2c_{GFz}{d_1}^2 + 4c_{GFy}h^2 + 2c_{GFz}{d_2}^2 & 0 \\ 0 & 0 & 0 & 4c_{SFy} \end{bmatrix} \tag{17}$$

The selection matrix T of the generalized forces is:

$$T = \begin{bmatrix} -4k_{GFy} & 0 & -4c_{GFy} & 0 & 1 & 0 \\ 0 & -4k_{GFz} & 0 & -4c_{GFz} & 0 & 0 \\ 4c_{GFy}h & 2k_{GFz}d_1 - 2k_{GFz}d_2 & -4c_{GFy}h & 2c_{GFz}d_1 - 2c_{GFz}d_2 & 0 & 0 \\ 0 & 0 & 0 & 0 & 1 & -1 \end{bmatrix} \tag{18}$$

In the state space formulation the equations of motion of the system can rewritten as:

$$\dot{X} = AX + BU \tag{19}$$

where the state vector X and the input vector U are:

$$X = \begin{Bmatrix} q & \dot{q} & y_G & z_G \end{Bmatrix}^T, U = \begin{Bmatrix} v_{Gy} & v_{Gz} & F_S & F_{act} \end{Bmatrix}^T \tag{20}$$

with A the state matrix, B the input matrix

$$A = \begin{bmatrix} 0 & I & 0 \\ -KM^{-1} & -CM^{-1} & TM^{-1} \\ 0 & 0 & 0 \end{bmatrix}, B = \begin{bmatrix} 0 \\ TM^{-1} \\ I \end{bmatrix} \tag{21}$$

The relationship between input and output can be represented as:

$$Y = CX + DU \tag{22}$$

where Y is the output vector, C the output matrix and D the feedthrough matrix

$$Y=\{v_S \quad v_F\}^T, C=\begin{bmatrix} 0 & 0 & 0 & 0 & 1 & 0 & -(z_{0F}+z_{0S}) & 1 & 0 & 0 \\ 0 & 0 & 0 & 0 & 1 & 0 & -(z_{0F}+z_{0S}) & 1 & 0 & 0 \end{bmatrix}, D=[0] \tag{23}$$

4. Control design & results

The control action is designed to achieve two main goals: active isolation of the payload from the ground disturbances and vibration damping during the machine work processes. These two actions allow to operate on the stage without external disturbances. The XZ and YZ are considered the same so the control laws along the two planes are equivalent.
Furthermore, from the control point of view, the adopted model is oversized respect to the control requirements if the goal is the isolation of the payload. As a matter of fact, in this case a two degrees of freedom model is sufficient while if also the dynamics of the frame is supposed to be controlled, then a 4 dof model is necessary.
The considered system can be considered as intrinsically stable due to the presence of mechanical stiffness between the payload and the frame allowing to obtain a negative real part for all the eigenvalues of the system.
Root loci of the system in open and closed loop configurations are reported in Figure 16.

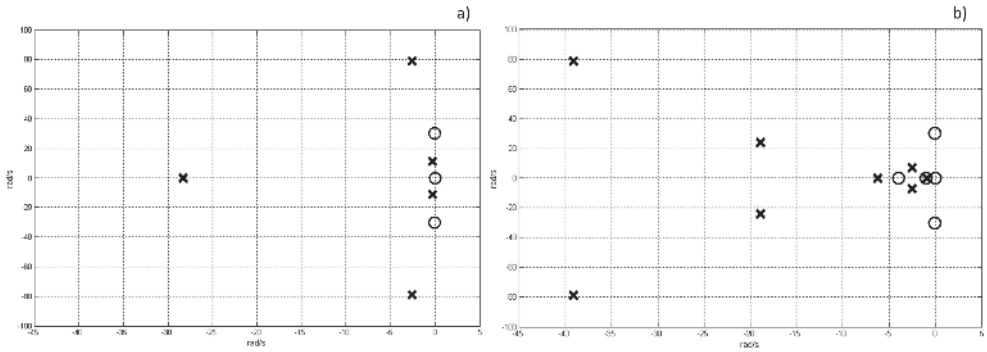

Fig. 16. Root loci of open loop (a) and closed loop (b) configurations (Circles: zeros; Crosses: poles).

Since the system along YZ (XZ) presents one actuation point and a couple of sensors (frame and stage velocities), a solution with a SISO control strategy is not feasible. A simplest solution to this problem considers the difference between the measured velocities as the feedback signal, so the system can be assumed as SISO and the control design becomes simpler.
Figure 17 shows that the system dynamics has a peak at 1.8 Hz related to the stage and higher modes related to the interaction of the stage with the frame and the ground at 10 Hz and beyond.
The control action is focused on damping the mode related to the stage by adding on the loop a lead-lag compensator.

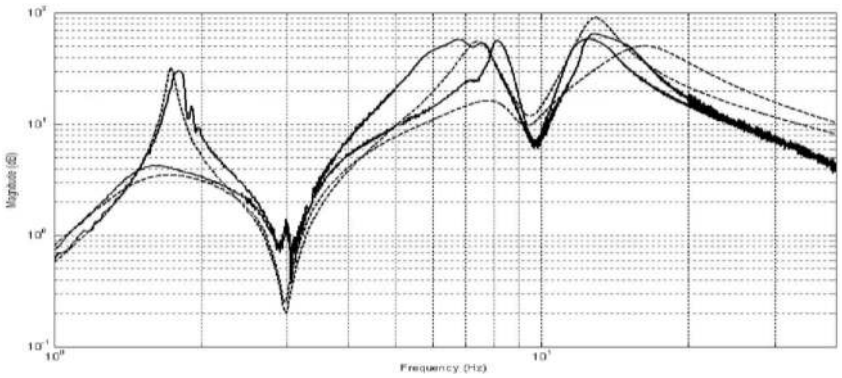

Fig. 17. Vibration damping action. Transfer function from the actuator force to the difference of frame and stage velocities ($(\dot{q}_S - \dot{q}_F)/F_{ACT}$). Open-loop vs Closed-loop. Solid line: experimental; Dashed line: numerical.

The two actions can be expressed as:

$$C_{LAG} = \frac{s + z_{LAG}}{s + p_{LAG}}$$
$$C_{LEAD} = \frac{s + z_{LEAD}}{s + p_{LEAD}} \tag{12}$$

The C_{LAG} action is used to improve the transient response at low frequency, while the C_{LEAD} is useful to increase the stability margin of the closed-loop system.

Therefore the resulting Lag-Lead action allows to compensate the geophone the critical phase behavior of the geophones and furthermore guarantees a quick damping action with good levels of stability margins.

The experimental tests have been performed to validate the two control actions. Figure 17 shows the frequency response function in open loop and closed loop, numerical and experimental calculated between the force of the actuator and velocity measured with the geophone on the stage. The force acts both on the stage and the frame, the dynamics of both the subsystems are visible. The vibration damping of the control action is validated on the stage mode (1.8 Hz peak) and the good correspondence between the simulated and experimental response is useful to validate the modeling approach.

A further demonstration of the correctness of the damping action is the velocity time response reported in Figure 18. In this case the system is excited with an impulse from the actuator and the velocity is measured on the stage. Numerical and experimental responses are superimposed to provide a further validation of the model (the position time response is not reported since the machine is not provided with displacement sensors and hence this validation could not be possible to perform). Figure 18.a shows open loop response, Figure 18.b shows closed loop response while in Figure 18.c the force exerted by the actuators is reported.

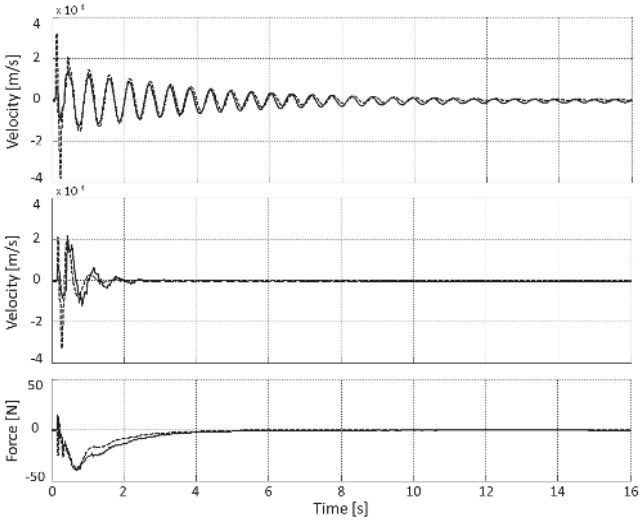

Fig. 18. Impulse time response, force from the actuator and velocity measured on the stage. Open-loop (a), Closed-loop (b), Force exerted by the actuators. Solid line: experimental results. Dashed line: numerical results.

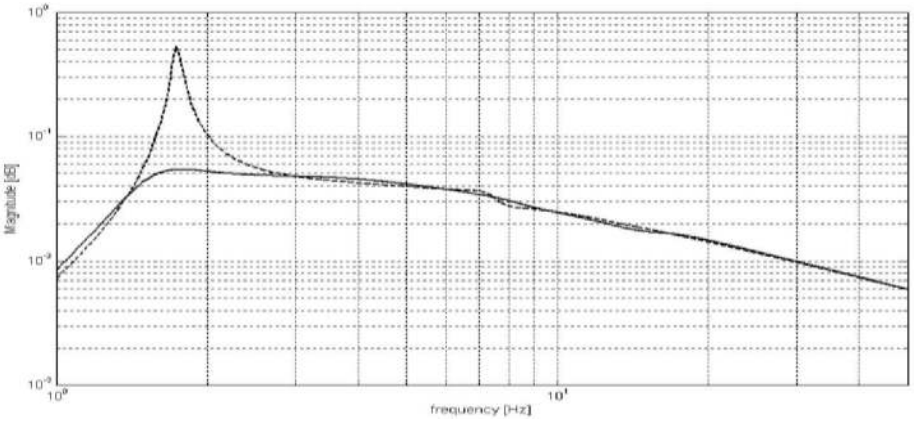

Fig. 19. Vibration damping action. Transfer function from a force applied on the stage to the velocity measured on the stage $\left(\dot{q}_S / F_{STAGE}\right)$. Numerical response. Solid line: closed-loop; Dashed line: Open-loop.

The excitation coming from the laser-axis action on the payload is controlled in an effective way as shown in Figure 19 where the numerical transfer function between a force impulse on the stage and the related measured velocity is reported.
The active isolation action is verified by simulating the excitation coming from the ground. The experimental test in this case has not been performed since in reality it is difficult to excite the machine from the ground in a controlled and effective way. Nevertheless the

model is reliable as proved in Figure 15 and the obtained results can be assumed as a good validation of the control action.
Figure 20 illustrates that the closed loop system is capable to reject the disturbances coming from the ground in an effective way.

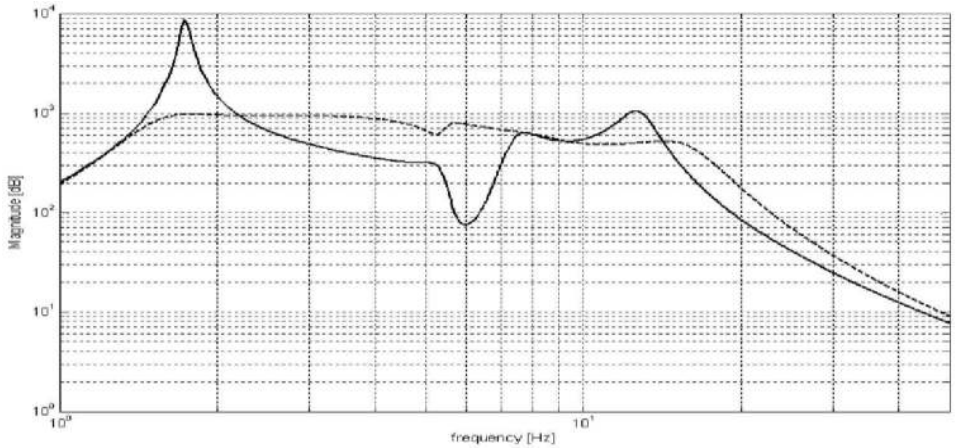

Fig. 20. Active isolation action. Transfer function from a simulated ground velocity to the velocity measured on the stage $(\dot{q}_S/\dot{q}_G)$. Numerical response. Solid line: Open loop configuration. Dashed line: Closed loop configuration.

5. Conclusions

In this chapter the realization of an active isolation and damping of vibrations for high precision laser cutting machine has been illustrated.
The literature analysis confirms that in the last decades active configurations had an exponential growth due to their high performance level.
The proposed solution uses Lorentz type electromagnetic actuators since they can be easily integrated in the mechanical structure and allow to reach good results.
A mechatronic approach has been used to manage the criticalities introduced by the subsystems interactions since it provides an overall view of the system.
A 4 degrees of freedom model has been carried out by means of Lagrange equations approach and was used to choose and set the control strategy. The proposed control technique is a lead-lag compensator able to control the stage dynamics and isolate it from the external disturbances.
The effectiveness of the vibration damping and the active isolation actions have been validated experimentally by analyzing the plant behavior in open-loop and closed-loop configurations with frequency and time responses. The results have been compared to the numerical computations to prove the correctness of the modeling approach.
Future works will be focused on the tests of new control strategies and on the evaluation of the adopted solutions compared to existing methods.

6. References

Anderson E., Leo D.J., Holcomn M.D, (1996). UltraQuiet platform for active vibration isolation, Proceedings Smart Structures and Integrated Systems 2717, San Diego, CA, pp. 436–451.

Beadle B.M., Hurlebaus S., Gaul L., Stöbener U. (2005). Active control strategies for vibration isolation, in Proc. IUTAM Symp. Vibration Control of Nonlinear Mechanisms and Structures 2005, Munich, Germany, pp. 91-100.

Brusa E., Carabelli S., Genta G., Maddaleno F., Silvagni M., Tonoli A. (2001). Voice coil actuator for Active Vibration Isolation in Microgravity, 6th ISMST, Torino.

Crede, C. (1951). Vibration and shock isolation, John Wiley and Sons Inc., New York, USA

Elliott S.J. (2001). Signal processing for active control, Academic Press.

Hauge, G.S. Campbell, M.E.. (2004). Sensors and control of a space-based six-axis vibration isolation system. Journal of Sound and Vibration 269. Pp 913–931.

Huan, S. L., & Pater, A. R. (1985). Analysis and prediction of geophone performance parameters. Geophysics, 50(8), 1221:1228.

Hyde T.T, (1997) An experimental study of active isolation. Proceedings of the 38th AIAA/ASME/ASCE/AHS/ASC, Structures, Structural Dynamics and Materials Conference, Orlando, FL, pp. 1763–1773.

Kuo S.M., Morgan D.R., (1996). Active noise control systems: algorithms and DSP implementations, John Wiley & Sons.

Preumont, A. (2002). Vibration control of Active Structures. Kluwer Academic Publishers, 2nd Edition, Netherlands

Riedesel, M., Moore, R. D., & Orcutt, J. A. 1990. Limits of Sensitivity of Seismometers with Velocity Transducers and Electronic Amplifiers. Bulletin of the Seismological Society of America, 80(6), 1725:1752.

Rivin, E. I. (1979). Principles and criteria of vibration isolation of machinery. Trans. of the ASME, Journal of Mechanical Engineering, 101:682–692.

Sullivan J., Rahman Z., Cobb R., Spanos J. (1997). Closed-loop performance of a vibration isolation and suppression system, Proceedings of the American Control Conference, Vol. 6, Albuquerque, NM, pp. 3974–3978.

Thayer, D., Vagners, J., von Flotow, A., Hardham, C. and Scribner, K., (1998). "Six Axis Vibration Isolation Using Soft Actuators and Multiple Sensors," Proceedings of the 21st Annual AAS Guidance and Control Conference, Feb 1998.

Thomson, W. (1971). Theory of vibration with applications. George Allen and Unwin.

Watters B.G., Coleman R.B., Duckworth G.L., Berkman E.F. (1988). A perspective on active machinery isolation, Proceedings of the 27th Conference on Design and Control, Vol. 3, Austin, TX, pp. 2033–2038.

Vibration Analysis and Control - New Trends and Developments
Edited by Dr. Francisco Beltran-Carbajal

ISBN 978-953-307-433-7
Hard cover, 352 pages
Publisher InTech
Published online 06, September, 2011
Published in print edition September, 2011

This book focuses on the important and diverse field of vibration analysis and control. It is written by experts from the international scientific community and covers a wide range of research topics related to design methodologies of passive, semi-active and active vibration control schemes, vehicle suspension systems, vibration control devices, fault detection, finite element analysis and other recent applications and studies of this fascinating field of vibration analysis and control. The book is addressed to researchers and practitioners of this field, as well as undergraduate and postgraduate students and other experts and newcomers seeking more information about the state of the art, challenging open problems, innovative solution proposals and new trends and developments in this area.

INTECH
open science | open minds

InTech Europe
University Campus STeP Ri
Slavka Krautzeka 83/A
51000 Rijeka, Croatia
Phone: +385 (51) 770 447
Fax: +385 (51) 686 166
www.intechopen.com

InTech China
Unit 405, Office Block, Hotel Equatorial Shanghai
No.65, Yan An Road (West), Shanghai, 200040, China
中国上海市延安西路65号上海国际贵都大饭店办公楼405单元
Phone: +86-21-62489820
Fax: +86-21-62489821